THE ASTROPHYSICAL JOURNAL, 226:937–946, 1978 December 15

AN OBSERVATIONAL STUDY OF THE ECLIPSING BINARY RZ OPHIUCHI*

BARROW W. BALDWIN
University of Victoria, British Columbia
Received 1977 December 6; accepted 1978 June 27

ABSTRACT

Orbital elements are derived from new spectroscopic and photometric observations. The masses and radii are inconsistent with evolutionary tracks for single stars, but neither star fills its Roche lobe. Analysis of the circumstellar Balmer emission lines indicates that the primary is surrounded by an extensive, highly flattened disk of nonuniform density. The velocity gradient in the disk is steeper than that expected from Keplerian motion.

Subject headings: stars: eclipsing binaries — stars: individual

I. INTRODUCTION

RZ Oph (BD +7°3832) is a long-period eclipsing binary that displays circumstellar hydrogen emission lines throughout its orbital cycle. Only two light curves, both based on visual observations, have been published (Seares 1908; Nijland 1908). Shapley (1913) computed a provisional orbit for the system based on the mean of these two light curves, but there are such large differences between them that Shapley's orbital elements should be viewed with suspicion.

The most recent radial-velocity study is that of Hiltner (1946). From 37 120 Å mm^{-1} plates obtained during one cycle he found a velocity range of 28 km s^{-1}, but there was no discernible correlation with phase, probably due to line blending at low dispersion. He also studied the double emission components at Hβ and found that they underwent an eclipse similar to that in other binaries with Balmer emission (e.g., RW Tau).

II. PHOTOMETRIC OBSERVATIONS

Photoelectric observations were made by the author with the University of Victoria's 30 cm telescope during primary eclipses in 1973 September and 1974 May. V and B filter measurements were made differentially with respect to BD +6°3917 and BD +6°3918 in standard fashion, with observations of the variable being bracketed by observations of the comparison stars and the sky. A fuller description of the observing procedure and the equipment used is given by Baldwin (1976). The observations are summarized in Table 1. No correction has been made for differential extinction because the corrections are an order of magnitude smaller than the standard errors of the observations. The origin of the large scatter in the B filter observations inside eclipse is not instrumental, as can be seen by comparing the values of Δm(BD +6°3918 − BD +6°3917) obtained during eclipse. The Balmer emission-line strength is variable

TABLE 1

PHOTOMETRIC OBSERVATIONS OF RZ OPHIUCHI

Time (JD$_{geo.}$ 2,440,000+)	Δm (RZ Oph − BD +6°3917)	Δm (BD +6°3918 − BD +6°3917)
	V Filter	
1936.7168	0.57	−0.13
1937.6925	1.11	−0.16
1938.6717	1.07	−0.19
1940.6635	1.08	−0.09
1941.6706	1.11	−0.15
1950.6526	0.38	−0.11
1952.6645	0.34	−0.16
1953.6398	0.37	−0.12
2195.8762	0.42	−0.17
2197.8797	0.44	−0.12
2198.8451	0.77	−0.16
2206.8707	1.18	...
2209.7700	0.60	−0.19
2210.8577	0.40	−0.15
2211.8571	0.42	−0.16
2216.8830	0.44	...
	B Filter	
1936.7149	1.25	+0.48
1937.6905	2.05	+0.61
1938.6762	2.31	+0.44
1940.6689	2.18	+0.47
1941.6724	2.45	+0.49
1950.6563	0.74	+0.51
1952.6662	0.81	+0.48
1953.6418	0.75	+0.49
2195.8806	0.86	+0.47
2197.8732	0.85	+0.45
2198.8485	1.57	+0.43
2206.8746	2.36	...
2209.7730	1.21	+0.39
2210.8625	0.81	+0.46
2211.8290	0.78	+0.44
2216.8935	0.79	...

NOTES.—Δm_v (3918 − 3917) = −0.15 ± 0.01 mag (s.e.); Δm_B (3918 − 3917) = +0.47 ± 0.01 mag.

* Dominion Astrophysical Observatory Contribution No. 386 = NRC No. 16868.

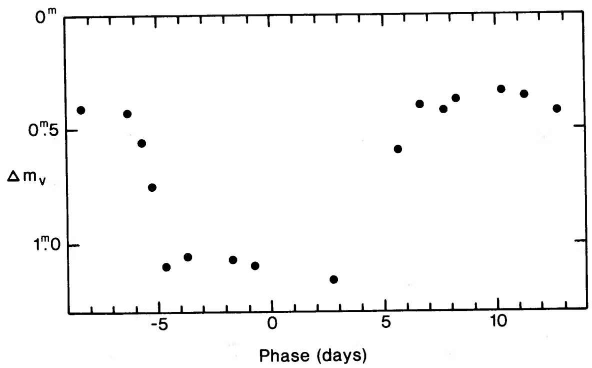

FIG. 1.—Combined V-filter values of Δm (RZ Oph − BD +6°3917).

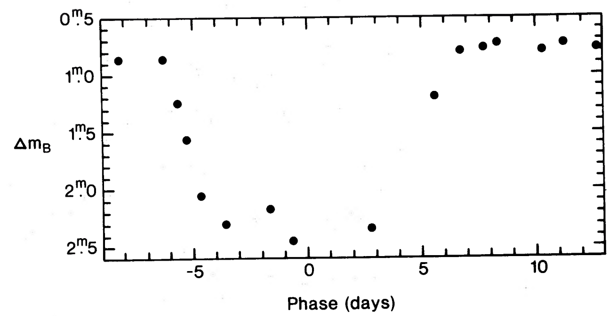

FIG. 2.—Combined B-filter values of Δm (RZ Oph − BD +6°3917).

during eclipse, but the effect is not large enough to account for the observed B magnitude differences. More photometry is needed in order to confirm this intrinsic variability and determine its cause.

The 1973 and 1974 observations were combined graphically by superposing and shifting them until the respective phases of maximum, minimum, and changing light coincided. The light curves are illustrated in Figures 1 and 2. Although the observations are insufficient to merit an orbital solution, some important information can be derived:

$$\text{depth of eclipse} = 0.71 \pm 0.05 \text{ mag } (V);$$
$$1.47 \pm 0.15 \text{ mag } (B);$$
$$\text{duration of totality} = 9^{\rm d}.3 \pm 0^{\rm d}.2;$$
$$\text{duration of each partial phase} = 1^{\rm d}.5 \pm 0^{\rm d}.2.$$

The uncertainties in the times were estimated visually. The uncertainties in the depths are based on the photometric errors within totality and outside eclipse. The eclipse depths agree within the errors with those found by Popper (1975) in the 1950s.

Times of minima were derived from each set of observations by fitting the composite curve to them and reading off the time corresponding to zero phase. This procedure is hazardous, but the results should certainly be accurate to $0^{\rm d}.2$. These have been listed in Table 2 along with others taken from the literature. A least-squares fit of the data in Table 2 to a linear ephemeris gave

$$T_{\rm min} = \text{JD } 2{,}442{,}204.39\ (\pm 0^{\rm d}.20) + 261^{\rm d}.9277\ (\pm 0^{\rm d}.0029)E,$$

where E is the cycle number and T_0 is an initial epoch. The values of E and $(O - C) = T_{\rm min}(\text{obs}) - T_{\rm min}(\text{calc})$ are listed in Table 2 and are plotted in Figure 3. Since $\langle (O - C) \rangle_{\rm rms} = 0^{\rm d}.37$, which is comparable to the uncertainty of a single determination,

TABLE 2

TIMES OF MINIMA AND (OBSERVED − CALCULATED) VALUES FOR RZ OPHIUCHI

$T_{\rm min}$(JD)	E	$O - C$ (days)	Reference
2,417,845.2.......	−93	+0.1	Beyer 1928
845.0.......	−93	−0.1	Zinner 1932
844.7.......	−93	−0.1	Seares 1908
18,106.7.......	−92	−0.3	Seares 1908
106.5.......	−92	−0.3	Nijland 1908
630.8.......	−90	−0.1	Nijland 1910
892.8.......	−89	0.0	Nijland 1931
19,154.2.......	−88	−0.6	Nijland 1931
678.8.......	−86	+0.2	Nijland 1931
940.2.......	−85	−0.3	Nijland 1931
20,464.0.......	−83	−0.4	Nijland 1931
988.7.......	−81	+0.5	Nijland 1931
21,512.4.......	−79	+0.3	Nijland 1931
22,822.4.......	−74	+0.7	Nijland 1931
23,345.3.......	−72	−0.3	Nijland 1931
23,606.9.......	−71	−0.6	Nijland 1928
24,393.4.......	−68	+0.7	Beyer 1928
655.6.......	−67	+0.4	Szafraniec 1960
655.5.......	−67	+0.3	Nijland 1927
25,179.3.......	−65	+0.2	Beyer 1928
179.5.......	−65	+0.4	Szafraniec 1962
440.3.......	−64	−0.7	Nijland 1929
26,277.0.......	−61	+0.2	Nijland 1931
488.5.......	−60	−0.2	Nijland 1932
489.2.......	−60	+0.5	Graff 1931
27,012.5.......	−58	−0.1	Nijland 1933
274.9.......	−57	+0.4	Nijland 1934
28,060.7.......	−54	+0.4	Nijland 1936
32,774.7.......	−36	−0.3	Szafraniec 1962
34,608.38......	−29	−0.1	Szafraniec 1959
41,942.3.......	−1	−0.2	Baldwin (this paper)
42,204.1.......	0	−0.3	Baldwin (this paper)

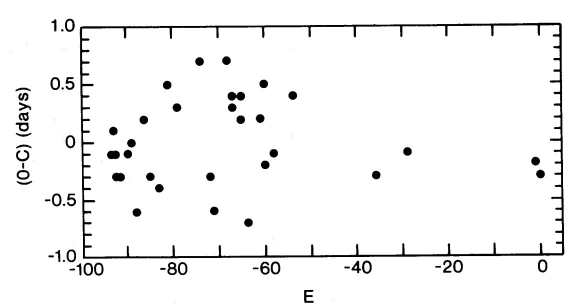

FIG. 3.—$(O - C)$ diagram for RZ Oph

there is no evidence for a period change, a conclusion which Koch (1970) also reached.

III. RADIAL VELOCITY MEASUREMENTS

Twenty-five spectrograms of RZ Oph were obtained with the 1.8 m telescope of the Dominion Astrophysical Observatory (DAO) from 1973 July to 1975 October. The spectrum outside eclipse is similar to that of α Per (F5 Ib). There is strong double emission at Hα and Hβ, and at Hγ it is present but does not rise above the continuum. There is also a trace of emission at Hδ. The calcium K line is strong and sharper than its counterpart in the spectrum of α Per. The Mg II 4481 Å line was found to be anomalously weak and diffuse; the same effect was looked for in other lines that arise from nonmetastable levels, but with inconsistent results. The spectrum inside eclipse is very similar to that of ξ Cyg (K5 Ib). In addition, there is strong double emission at Hβ and Hγ. During eclipse the 4481–4482 Å feature is normal.

The radial velocity measurements are summarized in Table 3. Spectrograms were obtained with three different gratings; for the 15 Å mm^{-1} and 60 Å mm^{-1} plates, lines suitable for radial velocity measurement in late-type spectra had already been determined (Batten *et al.* 1971) and were used in this study. For the 30 Å mm^{-1} plates, suitable lines were chosen from a list used at the DAO in the past with prism spectrographs giving a similar dispersion. All the plates were measured with ARCTURUS, the oscilloscope measuring device at the DAO. A more detailed description of the measurement and reduction techniques, and a list of individual line velocities, is given elsewhere (Baldwin 1976). In general, for plates taken outside eclipse, 10 to 20 lines were measured, whereas for plates taken inside eclipse, only five to eight lines were used.

TABLE 3

RADIAL VELOCITY MEASUREMENTS FOR RZ OPHIUCHI

Time of Mid-Exposure (geocentric JD 2,440,000+) (1)	Dispersion (Å mm^{-1}) (2)	Primary $V_{\odot}$ (km s^{-1}) (3)	Secondary $V_{\odot}$ (km s^{-1}) (4)
1896.9107.....	60	+3.1 ± 8.1 (s.e.)	−16.1
1908.7823.....	60	+15.6 ± 2.6	−12.0
1931.7274.....	60	+7.9 ± 3.0	−30.8
1938.7014.....	60	...	−13.3 ± 1.6
1939.7299.....	60	...	+5.2 ± 3.8
1940.7250.....	60	...	+9.7 ± 1.8
1957.6566.....	60	+5.6 ± 2.0	+23.7
2195.9177.....	30	−11.6 ± 1.4	−20.0
2195.9417.....	30	−9.8 ± 1.1	−34.6
2203.8986.....	30	...	−3.2 ± 1.4
2205.8726.....	30	...	−3.0 ± 2.1
2206.8799.....	30	...	+2.1 ± 1.3
2207.8694.....	30	...	+1.3 ± 1.8
2208.8997.....	30	...	0.0 ± 1.9
2216.9181.....	15	−0.3 ± 2.5	+10.1
2226.8017.....	15	−1.3 ± 1.3	+19.4
2228.8510.....	15	−3.4 ± 0.6	+23.5
2254.7885.....	15	−8.0 ± 0.7	+41.2
2265.7823.....	15	−8.0 ± 0.8	+43.1
2274.7576.....	15	−10.2 ± 0.9	+40.9
2275.7833.....	15	−9.3 ± 1.1	+43.6
2315.6781.....	30	+1.2 ± 2.5	+18.1
2329.6713.....	30	+5.8 ± 1.7	+1.0
2607.8014.....	15	−6.8 ± 1.3	−26.3
2637.7698.....	15	+21.1 ± 0.8	−30.1

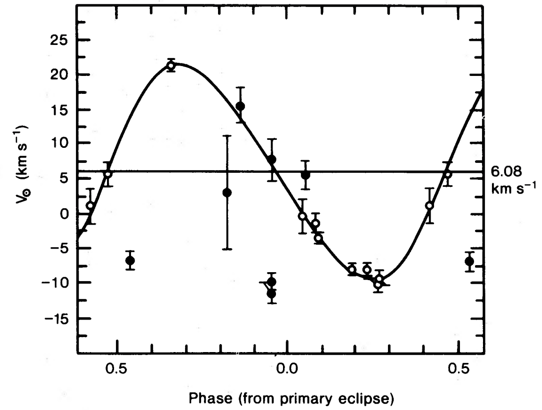

FIG. 4.—Radial velocities outside eclipse. Open circles represent points used to obtain the solution (*solid curve*). Other measures are indicated by closed circles; most were obtained at lower dispersion.

The velocity measures for the primary are illustrated in Figure 4. The solid curve represents the orbital solution calculated according to the Lehmann-Filhés method and is based on all 15 Å mm^{-1} and 30 Å mm^{-1} plates outside eclipse, except those at phases 0.969 and 0.542. The two measures at phase 0.969, just before the onset of primary eclipse, deviate badly from the run of the others and may be indicative of a "Zeta Aurigae effect" (Wright 1970). The velocity at phase 0.542 was rejected because it is obtained from a poorly exposed plate. The 60 Å mm^{-1} plate material was excluded because of its poorer quality. The orbital elements are listed in Table 4. Without excluding any plates, an orbital solution could still be obtained, with $K_1 = 10.3 \pm 2.8$ km s^{-1}. No statistically significant correlation between radial velocity and excitation potential was found in the individual line velocities.

There is no obvious evidence for the secondary in the spectra outside eclipse. Probably lines of the secondary are present but are blended irretrievably with lines of the primary; this may explain some of the peculiar velocities recorded. A careful examination of the Mg II 4481 Å region (actually a blend dominated by the Fe I 4482.2 Å line) on the 15 Å mm^{-1} plates

TABLE 4

ORBITAL ELEMENTS

$P = 261^{d}.9$ (assumed)

Element	Primary	Secondary
T (periastron)....	JD 2,442,069 ± 12 (s.e.)	2,442,030 ± 17
K (km s^{-1})......	15.3 ± 0.8	40.9 ± 2.2
e..............	0.10 ± 0.09	0.11 ± 0.05
ω..............	273° ± 16°	33° ± 24°
V_0 (km s^{-1}).....	+6.1 ± 0.8	−0.5 ± 1.5

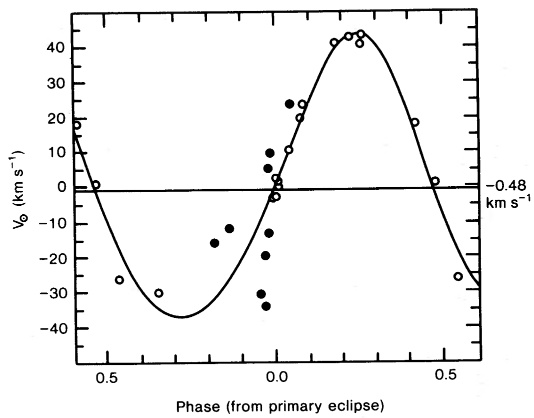

FIG. 5.—Radial velocities for RZ Oph (secondary). The symbols have the same meaning as those in Fig. 4.

revealed several interesting features: (1) The width of the line is much greater than that usually found for F5 supergiants but is comparable to that found for K5 supergiants. (2) The overall profile consists of a set of sharp components superposed on a broad, weak feature. Radial velocity measures of the wings of this line (i.e., the broad feature) from plates obtained outside eclipse are recorded in Table 3 (col. [4]) and illustrated in Figure 5. The coherent out-of-phase variation of velocity with phase indicates that the secondary is probably responsible for the feature. The velocities from the 60 Å mm^{-1} plates fall systematically above the others, perhaps because the effective wavelength is different at that dispersion. As before, the observations just preceding the onset of eclipse (i.e., at phase 0.969) fall inexplicably low.

The curve drawn in Figure 5 represents the orbital solution for the secondary based on all 15 Å mm^{-1} and 30 Å mm^{-1} plates (excluding the two at phase 0.969). The orbital elements are listed in Table 4. The orbital elements derived from the primary and secondary velocity curves are inconsistent in several respects. The most important difference occurs for the values of V_0. While this is not uncommon, it diminishes confidence in the solution. The values of ω and T are also inconsistent, but the differences are not alarming because of the small eccentricity.

For an assumed inclination of 90° the masses and dimensions are listed in Table 5. The radii were calculated from the durations of partial and total phases. It is interesting to compare these values with the corresponding radii of the Roche lobes, according to the approximate expression given by Plavec (1970): $(R_{\rm Roche})_1 = 121\ R_\odot$ and $(R_{\rm Roche})_2 = 77\ R_\odot$. The stars do not fill their Roche lobes, by a wide margin. Only for an inclination as low as 76° would the radius of the secondary equal that of its Roche lobe, and in that case the radius of the primary would be only 2 $R_\odot$.

TABLE 5

MASSES AND DIMENSIONS

$a_1 = 5.5\ (\pm 0.3) \times 10^7$ km ($i = 90°$ assumed)
$a_2 = 14.7\ (\pm 0.8) \times 10^7$ km
$a = 290 \pm 13\ R_\odot$
$M_1 = 3.5 \pm 0.4\ M_\odot$
$M_2 = 1.3 \pm 0.1\ M_\odot$
$R_1 = 5 \pm 1\ R_\odot$
$R_2 = 34 \pm 3\ R_\odot$

IV. THE EVOLUTIONARY STATUS OF RZ OPHIUCHI

If RZ Oph were in a state of pre–main-sequence contraction (without mass exchange) it might be possible to explain the origin of the circumstellar material, even though neither star currently fills its Roche lobe. However, Roxburgh's (1966) technique can be used to show that this hypothesis is inconsistent with the masses and radii of the components. The age of the primary can be computed from its mass and radius and Iben's (1965) evolutionary tracks. Assuming the same age for the secondary, one can show that for its mass its radius is nearly 10 times larger than it should be. Pre–main-sequence evolutionary calculations incorporating the effects of mass transfer have been made (e.g., Yamasaki 1971), but in a rather arbitrary way. If one assumes that RZ Oph did not start out as a contact system, and that the mass transfer rate was not sufficiently large to invert the mass ratio, then published calculations suggest that the discrepancy would be even worse.

The same method can be used to analyze the consistency of the alternative hypothesis, that RZ Oph is in a state of post–main-sequence evolution as a detached system. One finds that the expected radius of the secondary is only 1.1 $R_\odot$, which is smaller by a factor of 31 than the actual radius.

Therefore the components of RZ Oph cannot have evolved in the normal manner of single stars, and so the configuration must be the result of mass exchange. The system SX Cas may be analogous. Neither of its components appears to fill its Roche lobe (Andersen 1973), yet emission is always present in its spectrum. Outside eclipse the spectrum resembles that of an A supergiant, except that the Mg II 4481 Å line and certain other dilution-sensitive lines are weak (Struve 1944).

An evolutionary scheme involving mass exchange in a semidetached system, followed by the onset of core helium burning in the secondary and subsequent detachment from its Roche lobe, should be considered, but since little theoretical work has been done for binaries with giant and supergiant primaries (Plavec 1968*a*), evolutionary calculations are required in order to investigate the question in detail.

V. SPECTROPHOTOMETRY OF THE EMISSION LINES

Rectified intensity tracings were derived from the spectrograms in standard fashion (Baldwin 1976). In order to study the circumstellar emission-line profiles, it is necessary to subtract out the underlying stellar absorption spectrum. This procedure is valid if the circumstellar material is optically thin; otherwise, the combined spectrum should be analyzed. However,

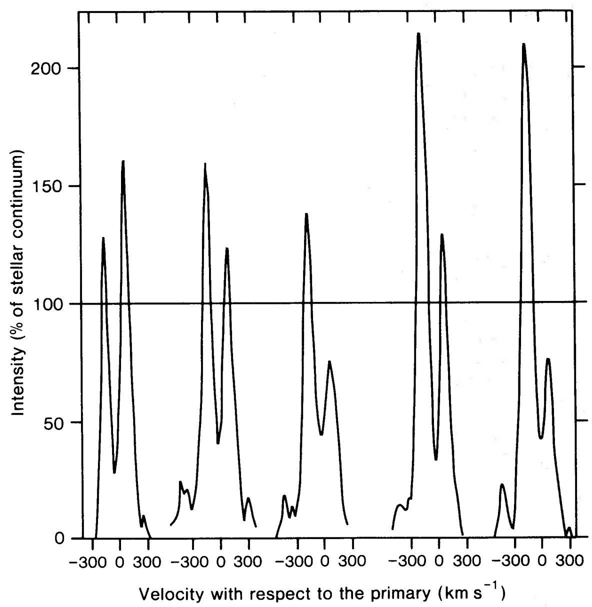

FIG. 6.—Sample Hβ emission line profiles during eclipse. From left to right: phase 0.999, 0.007, 0.011, 0.014, and 0.018.

that would require a theoretical treatment not yet developed.

Plates of a number of late-type supergiants were obtained, and several comparison stars were found to reproduce satisfactorily the underlying absorption spectrum of RZ Oph. For the plates of RZ Oph taken outside eclipse, two comparison stars, α Per and HR 7834, were used. For those taken inside eclipse the comparison star was ξ Cyg. At Hγ and Hδ the emission was weak, and at the calcium H and K lines it was poorly determined because of inaccurate spectrophotometry. The most reliably determined profiles are those at Hβ (e.g., those in Fig. 6), and they have been used in the following analysis.

From the Hβ emission line profiles, velocities and equivalent widths were measured; they are recorded in Table 6. Since each profile consists of a redshifted and a blueshifted lobe, measures were made for each. The boundary between the lobes was chosen to lie at the wavelength corresponding to the orbital velocity of the primary, even though in some cases the intensity minimum between the lobes was slightly shifted from this position. The recorded velocities outside eclipse are with respect to the primary, and those inside eclipse are with respect to the secondary.

TABLE 6

Hβ EMISSION MEASUREMENTS

	RED COMPONENT		BLUE COMPONENT		
PHASE* (1)	EW (Å)† (2)	Velocity of Red Lobe (km s^{-1}) (3)	EW (Å)† (4)	Velocity of Blue Lobe (km s^{-1}) (5)	TOTAL EW (Å)‡§ (6)
0.827.........	2.34	+154	1.71	−108	4.05
0.872.........	1.85	+131	1.75	−116	3.60
0.960.........	1.70	+100	0.93	−139	2.63
0.969.........	1.93	+113	0.78	−99	2.71
0.969.........	1.92	+128	0.66	−74	2.58
0.986.........	5.20	+116	1.58	...‖	2.35
0.990.........	3.33	+108	1.30	−69	1.61
0.994.........	3.78	+131	2.01	−77	2.01
0.999.........	3.41	+104	2.21	−109	1.95
0.007.........	2.30	+104	3.18	−118	1.90
0.011.........	1.47	+84	2.89	−138	1.51
0.014.........	2.24	+79	5.05	−138	2.53
0.018.........	1.74	+89	5.02	−128	2.35
0.049.........	1.22	+91	2.00	−121	3.22
0.059.........	1.56	+100	1.76	−123	3.32
0.087.........	1.74	+109	1.58	−123	3.32
0.095.........	1.93	+104	2.31	−106	4.24
0.194.........	2.06	+89	2.19	−136	4.25
0.235.........	1.96	+101	2.43	−128	4.39
0.270.........	1.96	+104	2.48	−138	4.44
0.274.........	1.90	+94	2.19	−133	4.09
0.426.........	1.94	+94	2.17	−133	4.11
0.479.........	1.75	+84	2.79	−133	4.54
0.541.........	1.72	+104	1.78	−116	3.50
0.656.........	2.16	+113	1.90	−94	4.06

* Phase with respect to primary eclipse.

† With respect to the underlying stellar continuum.

‡ With respect to the continuum of the combined light of the system.

§ See discussion of conversion factor in § V.

‖ Not resolved.

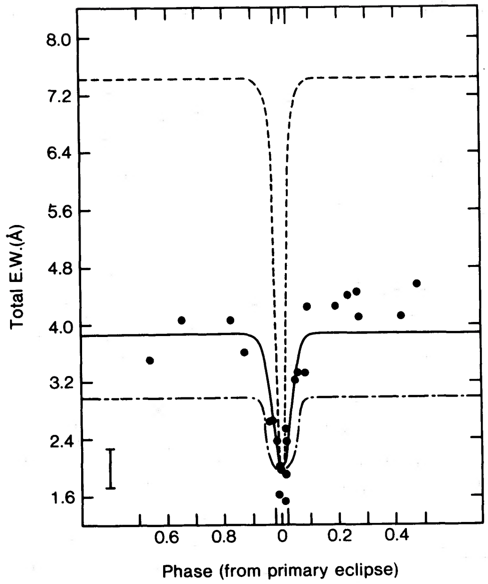

FIG. 7.—Equivalent width of Hβ emission versus phase. The circles indicate the observations, and the curves (normalized to 1.95 Å at phase 0.999) are derived from computer models for a disk of outer radius $r_0 = 0.4a$, with different values of m, the exponent in the power-law density distribution: —·—·, $m = 0$; ———, $m = -1$; ----, $m = -2$. The error bar represents twice the estimated uncertainty in any one measure. Primary eclipse is indicated by two vertical lines.

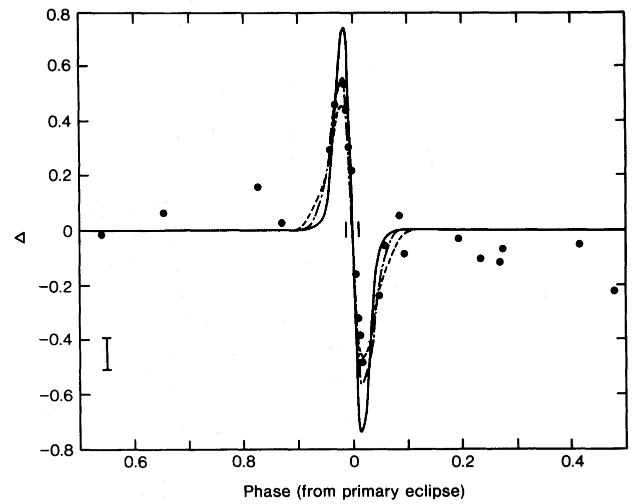

FIG. 8.—Relative strength of the Hβ emission lobes versus phase (Δ is defined in § V). The symbols have the same meaning as those in Fig. 7; for the computer models the density distribution is fixed ($m = -1$) and the outer radius of the disk (r_0) is varied: ———, $r_0 = 0.3a$; —·—·, $r_0 = 0.4a$; ----, $r_0 = 0.5a$.

The equivalent widths recorded in columns (2) and (4) of Table 6 are in units of the underlying stellar continuum, but the values of total equivalent width in eclipse (found in col. [6]) have been converted to units of the continuum of the combined light of the system by multiplying by the factor of $10^{-0.4\Delta m(\mathrm{H}\beta)}$, where $\Delta m(\mathrm{H}\beta)$ is the depth of primary eclipse at the wavelength of Hβ. By interpolating between the depths of eclipse measured with the B and V filters, one finds $\Delta m(\mathrm{H}\beta) \approx 1.15$ mag, which was used in reducing the equivalent widths to a common continuum level.

The variation of emission strength with phase is illustrated in Figure 7. This represents the light curve at Hβ of the circumstellar material. Although there is much scatter in the data, particularly during eclipse, it is clear that the emission strength decreases before the onset of eclipse, and after eclipse it continues to increase until about phase 0.10, after which it levels off.

The variation of the quantity

$$\Delta \equiv \frac{\text{EW (redshifted lobe)} - \text{EW (blueshifted lobe)}}{\text{EW (redshifted lobe)} + \text{EW (blueshifted lobe)}}$$

with phase has been plotted in Figure 8. During eclipse there is an almost linear red to blue variation from ingress to egress of the sort first noticed by Wyse (1934) in the eclipse spectrum of RW Tau. From phase 0.5 to primary eclipse the redshifted lobe is stronger and starts to increase in strength before the onset of eclipse. During the other half of the cycle the blueshifted lobe is stronger; at the end of eclipse it is at maximum strength, but afterwards its relative strength declines until about phase 0.10.

The equivalent widths of the emission at Hα, Hβ, Hγ, and Hδ relative to the underlying stellar continuum measured from plates taken near phase 0.27 are shown in Table 7. The Balmer decrement, $P_{\mathrm{em}}/P_{\mathrm{H}\beta}$, was computed by converting to power units and assuming that the underlying continuum can be represented by the sum of the radiation of two blackbodies with the dimensions given in Table 5 and temperatures appropriate for the spectral types. $P_{\mathrm{H}\beta}$ is then 1.33×10^{25} W. The values of $P_{\mathrm{em}}/P_{\mathrm{H}\beta}$ are given in Table 7. Limited information about the Balmer decrement at other phases is consistent with these values. There is no appreciable reddening effect for the observed Balmer decrement because Popper's (1975) colors of the components of RZ Oph, $(B - V)_{\mathrm{pr}} = +0.46$ and $(B - V)_{\mathrm{sec}} = +1.88$, are consistent with the observed spectral types.

VI. INITIAL MODEL OF THE CIRCUMSTELLAR MATERIAL

The behavior of the emission lines during eclipse is similar to that found in other systems for which circumstellar disks have been proposed (Batten 1970).

TABLE 7

THE BALMER DECREMENT (phase ≈ 0.27)

Line	Equivalent Width (Å)	$P_{\mathrm{em}}/P_{\mathrm{H}\beta}$
Hα..........	13.85	5
Hβ..........	4.09	1
Hγ..........	0.85	0.2
Hδ..........	≪0.7	≪0.1

Clearly, the circumstellar matter surrounds the primary, because the emission is visible at all phases yet weakens considerably during eclipse. Also, the motion in the disk must be predominantly that of direct rotation because of the observed red to blue variation during eclipse; for purely radial motion (e.g., an expanding atmosphere) Δ would remain constant throughout eclipse. Although evidence is scanty concerning the inner radii of circumstellar disks and their extent above and below the orbital plane (Batten 1970), it is usually assumed that the inner radius of the disk equals that of the central star and that the disk is highly flattened. Although the disk has some small extension above and below the orbital plane, the physical parameters within the disk will be assumed to be independent of distance above or below the orbital plane.

The outer radius of the disk can be estimated from Figures 7 and 8. After eclipse the emission strength does not fully recover until about phase 0.10. If this effect signals the end of the eclipse of the disk itself, then its outer radius must equal $r_0 = (\sin\theta + r_2)a = 0.47a$, where θ is the phase.

A rough estimate can also be made of the electron density by making some assumptions about the mechanism of energy production in the disk (Krzemiński and Kraft 1964). For pure hydrogen the total number of recombinations per second per cubic centimeter onto the fourth level is, assuming the temperature in the disk to be 6100 K (equal to that of the primary),

$$R_4 = 4.74 \times 10^{-14} N_e^2$$

(Cillié 1932), where N_e is the electron density (cm^{-3}). If one neglects recombinations onto higher levels and subsequent cascades and assumes that the only way of depopulating the level is by spontaneous emission, then

$$p_{42} h\nu_{42} \int_{\text{disk}} R_4 dV = P_{42}\,,$$

where P_{42} is the observed power emitted by the disk at Hβ and p_{42} is the relative probability of the transition from level 4 to level 2. The integration is taken over the volume of the disk, which can be approximated by the expression

$$V = \tfrac{1}{2} r_1^3 [\pi x^2 - \tfrac{1}{2}\pi - x^2 \sin^{-1}(1/x) - (x^2 - 1)^{1/2}]\,.$$

This represents the volume of a disk of inner radius r_1, outer radius xr_1, and thickness $\tfrac{1}{2}r_1$, with the effect of screening by the embedded star taken into account. For $x = 27$ (so $r_0 = 0.47a$), this leads to $V = 3.66 \times 10^{37}$ cm^3. For Hβ, the average equivalent width determined from the 15 Å mm^{-1} plates taken outside eclipse when there is no screening by the secondary is EW (Hβ) = 4.28 Å. Thus,

$$\int N_e^2 dV = 2.56 \times 10^{57}\ \text{cm}^{-3}\,.$$

If one defines the average electron density in the disk to be

$$\bar{N}_e = \left(\int N_e^2 dV/V\right)^{1/2},$$

then for Hβ, $\bar{N}_e = 8 \times 10^9$ cm^{-3}. Since cascades from levels higher than the fourth have been neglected, this value is actually an upper limit to the electron density.

VII. ANALYSIS AND CONCLUSIONS

Mihalas (1974) has pointed out that the general theoretical problem of calculating the spectrum emitted by a moving, extended atmosphere has not been solved. However, some progress has been made for the two limiting cases of negligible velocities and extreme velocity gradients, the latter case being of interest here. The escape-probability method for treating the transfer of radiation in a moving atmosphere was devised by Sobolev (1947, 1960) and has been applied to extended atmospheres (Castor 1970; Castor and Van Blerkom 1970) in which large velocity gradients dominate the process of photon diffusion.

For an atmosphere with a large velocity gradient, the solution (Sobolev 1947) of the equation of radiative transfer determines the energy, E_{ik}, emitted by the envelope per second per unit solid angle in the direction of the observer for the transition $k \to i$:

$$E_{ik} = A_{ki} h\nu_{ik} \int_{\text{envelope}} \beta_{ik} n_k dV\,, \qquad (1)$$

where

$$\beta_{ik} = \frac{1}{8\pi u\alpha_{ik}} \left|\frac{\partial V_z}{\partial z}\right| \left[1 - \exp\left(-2u\alpha_{ik} \Big/ \left|\frac{\partial V_z}{\partial z}\right|\right)\right]. \qquad (2)$$

Here A_{ki} = Einstein spontaneous emission coefficient, ν_{ik} = rest frequency of the line, n_k = number of atoms per unit volume in state k, u = mean thermal velocity of the atoms, α_{ik} = linear absorption coefficient, V_z = radial velocity of the volume element with respect to the observer, $\partial V_z/\partial z$ = gradient of the radial velocity in the direction of the observer. These expressions are valid only for velocity gradients large enough to satisfy the criterion

$$\Delta x = 2u \Big/ \left|\frac{\partial V_z}{\partial z}\right| \ll d_{\text{env}}\,, \qquad (3)$$

where d_{env} is the thickness of the envelope in the line of sight.

Two limiting cases will be considered here. For an optically thin envelope the expression for β_{ik} reduces to $\beta_{ik} = 1/4\pi$ and

$$E_{ik}(\text{thin}) = (1/4\pi) A_{ki} h\nu_{ik} \int n_k dV\,. \qquad (4)$$

For an optically thick envelope, the expression for

β_{ik} reduces to

$$\beta_{ik} = \frac{1}{8\pi u \alpha_{ik}} \left| \frac{\partial V_z}{\partial z} \right| \tag{5}$$

and

$$E_{ik}(\text{thick}) = A_{ki} h\nu_{ik} \int \frac{1}{8\pi u \alpha_{ik}} \left| \frac{\partial V_z}{\partial z} \right| n_k dV . \tag{6}$$

The equation of radiative transfer must be supplemented by the equations of statistical equilibrium in order to provide a complete description of the envelope. The problem is complex because the equations of statistical equilibrium contain the coefficients β_{ik}, which are themselves functions of the level populations. However, if the velocity gradient and electron temperature are known throughout the envelope, then in principle the equations can be solved at each point, and the emergent spectrum can be calculated. Here a simpler empirical technique will be used by assuming a power-law density distribution of the form

$$n_k = (n_k)_1 r^m \quad r_1 \leq r \leq r_0 , \tag{7}$$

where r is the distance from the center of the primary, and $(n_k)_1$ and m are variable parameters.

In general, the power emitted by the disk in a line depends not only on the density distribution, but also on the velocity distribution. However, if the disk is assumed to be optically thin in the line, then an enormous simplification takes place, because the effect of the density distribution is uncoupled from that of the velocity distribution. Since nothing is known about the velocity distribution in the disk, it is useful to consider at first an optically thin disk:

$$E_{ik}(\text{thin}) = (1/4\pi) A_{ki} h\nu_{ik} t (n_k)_1 \iint r^m dA . \tag{8}$$

Here t represents the thickness of the disk perpendicular to the orbital plane, and the integral is taken over those portions of the disk unobscured by either star.

Various models were computed using this expression, and it was found that the total emission strength is very sensitive to changes in m (see Fig. 7), the exponent of the power-law density distribution, whereas the relative strength of the emission lobes is especially sensitive to changes in the outer radius of the disk (see Fig. 8). The best fit will come from a combination of m and r_0 that balances these two effects. It was found visually that the best fit was obtained for $r_0 = 0.47a$, $m = -1.4$. However, there are systematic deviations that deserve attention: (1) At mideclipse $\Delta \approx +0.15$, whereas for a cylindrically symmetric disk it should be zero. In fact, the entire run of values during eclipse is anomalously displaced to the red. (2) Outside those phases where some of the disk is obscured by the secondary, one expects Δ to be constant and equal to zero. Yet during the phase interval $p = 0.1$–0.5 the observations are systematically "too blue," whereas just the opposite effect occurs during the interval $p = 0.5$–0.9. The uncertainties in the data are too small to encompass these systematic deviations, and the simplest explanation is that they are due to an asymmetry in the disk. Either the disk is larger on the trailing side, or the density is greater there. Computer models incorporating the first possibility indicated that in order to match the values of Δ inside eclipse the extent of the disk on the trailing side of the primary would have to be increased to $0.55a$, which is inconsistent with the phase at which the eclipse of the disk ends. Accordingly, this model was ruled out. The other possibility was incorporated into the model by using two values of m: m_t for the trailing side and m_l for the leading side. The best fit, for the values $r_0 = 0.47a$, $m_t = -1.3$, $m_l = -1.4$, is illustrated in Figures 9 and 10.

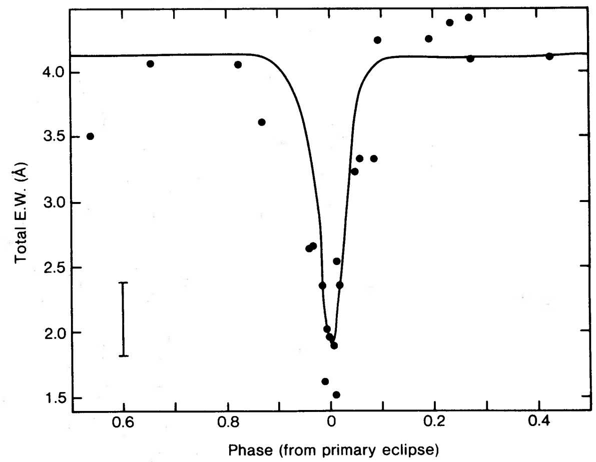

FIG. 9.—Equivalent width of Hβ emission versus phase for a transparent rotating disk (normalized to 1.95 Å at phase 0.999)—the best fit with $r_0 = 0.47a$, $m_t = -1.3$, $m_l = -1.4$.

The parameters m_t and m_l describe the density distribution of atoms in state k. The electron density can be related to that of n_k through the solution of the equations of statistical equilibrium for a transparent

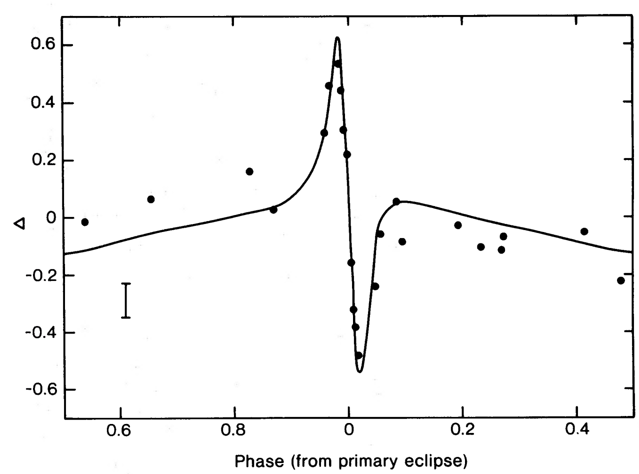

FIG. 10.—Variations of Δ (defined in § V) with phase for a transparent rotating disk—the best fit with $r_0 = 0.47a$, $m_t = -1.3$, $m_l = -1.4$.

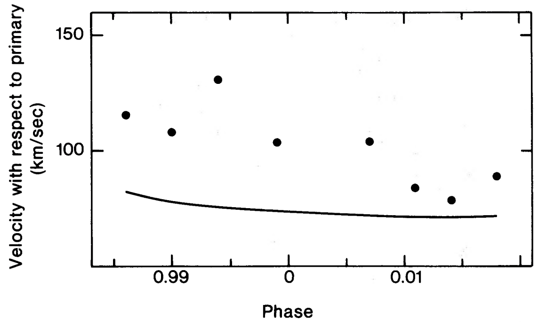

FIG. 11.—Computed velocities in the disk—the redshifted lobe. The circles represent the observations.

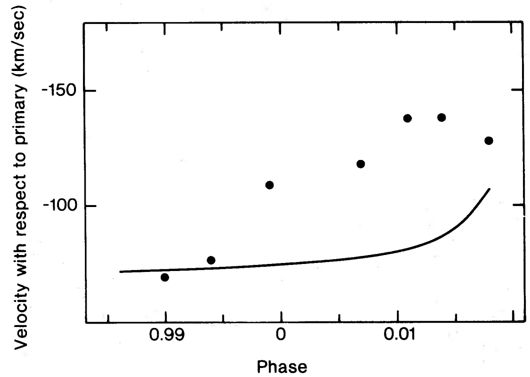

FIG. 12.—Computed velocities in the disk—the blueshifted lobe. The circles represent the observations.

envelope. The solution (Cillié 1936) consists of values of $Z_k = n_k/n_e n_+$ (n_+ = number of ions per unit volume) for various energy levels and temperatures. However, for any given energy level the temperature dependence is almost negligible, so that in the first approximation one can write Z_k = constant within the envelope. If $n_k \propto r^m$, then $n_e \propto r^{m/2}$ for a gaseous disk composed solely of hydrogen. For $m_t = -1.3$, $n_e \propto r^{-0.65}$ (trailing side), and for $m_l = -1.4$, $n_e \propto r^{-0.7}$ (leading side).

An attempt was made to derive some information about the velocity distribution in the disk by calculating velocities expected from a disk of outer radius $r_0 = 0.47a$ with a density distribution characterized by $m_t = -1.3$, $m_l = -1.4$. If one assumes that the measured velocity of the emission line profile is an average of all the line-of-sight velocities in the disk, each weighted by its contribution to the overall profile, then one can compute the velocity of each lobe using the expression

$$\bar{V} = \iint V_z n_k dA \Big/ \iint n_k dA \,, \tag{9}$$

where V_z is the radial velocity of the element, and the integration covers all the unobscured areas of the disk with positive (negative) radial velocity for the redshifted (blueshifted) lobe. The computed velocities during eclipse for Keplerian motion are illustrated in Figures 11 and 12. Because the computed velocities fall short of the observed ones, it is tempting to suppose that the mass of the primary (M_1) is too low. The computed curves would overlap the observations if M_1 were increased by a factor of 1.77, although it is impossible to match the slope of the observed run of velocities, particularly for the blue-displaced lobe. Clearly, the velocity structure is asymmetric on either side of the disk, and the velocity gradient in the disk is steeper than that expected on the basis of Keplerian rotation. It is also possible that the observed velocity behavior in the blueshifted lobe during egress indicates some leveling off of the velocity gradient near the star.

The results obtained so far have been based on the assumption of optical transparency in Hβ, yet it is not obvious that this should automatically be the case for RZ Oph. The disk is large, and there is some evidence of shell absorption effects in the spectrum outside eclipse. However, the observed Balmer decrement is very steep, and this behavior is usually associated with optical transparency. The arguments are not conclusive, but on balance the envelope is more likely to be transparent in Hβ. Nevertheless, models were computed for an optically thick disk using the expressions derived from the escape-probability method. Since this method is not valid for the analysis of radiation coming from that portion of the disk directly in front of the primary (because the velocity gradient is zero there), the analysis was restricted to the observations obtained during the total phase of eclipse. Plavec (1968*b*) made a similar analysis of the eclipse spectrum of RW Tau, and his expressions for the absorption coefficient and the Keplerian velocity gradient were used, even though the velocity distribution in the disk of RZ Oph is not entirely Keplerian. The details of this calculation have been given elsewhere (Baldwin 1976). In order to match the slope of the run of the observations in the Δ-phase plane it was again necessary to set the outer radius of the disk equal to $0.47a$. It is interesting to note that this is just equal to the size of the Roche lobe of the primary. It was also necessary to introduce an asymmetry in the disk similar to that required for the transparent disk in order to obtain a good fit to the observations.

If the disk is assumed to be transparent in Hβ, its thickness can be estimated. The total power emitted by the disk in the line at phase 0.999 was calculated to be

$$P_{\mathrm{H}\beta} = 1.246 \times 10^{20} t (n_4)_{\mathrm{in}} \quad \mathrm{ergs\ s^{-1}} \,,$$

where $(n_4)_{\mathrm{in}}$ is the density of atoms in level 4 (cm^{-3}) at the inner edge of the disk and t is its thickness (cm) perpendicular to the orbital plane. At phase 0.999 the observed equivalent width of the line is 5.62 Å. However, the run of the observations is not well defined during eclipse, and visual inspection suggests that a slightly lower value of 5 Å is more appropriate. Using this value, and assuming that the secondary radiates like a blackbody at a temperature of 3400 K, with radius 34 $R_\odot$, one can calculate the power emitted in the line:

$$P_{\mathrm{H}\beta} = 8 \times 10^{31} \quad \mathrm{ergs\ s^{-1}} .$$

Thus,

$$t(n_4)_{\mathrm{in}} = 6.4 \times 10^{11} \quad \mathrm{cm^{-2}} .$$

One can relate $(n_4)_{\mathrm{in}}$ to $(N_e)_{\mathrm{in}}$, the electron density at the inner edge of the disk, by using the solution to the equations of statistical equilibrium for a transparent envelope (Cillié 1936). For a disk composed solely of hydrogen at a temperature of 6100 K (corresponding to the surface of the primary), one finds

$$(n_4)_{\mathrm{in}}/(N_e)_{\mathrm{in}}^2 = 5.21 \times 10^{-21} \quad \mathrm{cm^3} .$$

The initial estimate of electron density in the envelope was $\bar{N}_e \approx 8 \times 10^9$ cm^{-3}. Since $N_e \propto r^{-0.675}$, the electron density at the inner surface of the disk can be found by integrating this function over the disk:

$$(N_e)_{\mathrm{in}} \approx 5 \times 10^{10} \quad \mathrm{cm^{-3}} .$$

Consequently, $(n_4)_{\mathrm{in}} \approx 13$ cm^{-3} and $t \approx 4.9 \times 10^{10}$ cm $= 0.002a$. The disk is highly flattened indeed, with a thickness perpendicular to the orbital plane of less than 1% of its diameter.

A lower limit to the mass of the disk can be found by assuming that the gas consists completely of ionized hydrogen. Then

$$M_{\mathrm{disk}} \geq \pi(r_0^2 - r_1^2)t\bar{N}_e m_{\mathrm{H}} ,$$

where m_{H} is the mass of the hydrogen atom. With $r_0 = 0.47a$, $r_1 = 0.016a$, $t = 0.002a$, $a = 290\ R_0$, and $\bar{N}_e = 8 \times 10^9$ cm^{-3}, this yields

$$M_{\mathrm{disk}} \geq 1 \times 10^{-10}\ M_\odot .$$

This value is similar to that found for disks in Algol-type systems but is much lower than that found for envelopes in long-period systems such as VV Cep (Batten 1973).

Clearly, much work remains to be done on the system. The simple computer models described here have proved useful in making a first estimate of the physical characteristics of the circumstellar material, although certain problems remain. Just outside eclipse the fit to the observations is poor; e.g., in Figure 9 the computed curve lies significantly higher than the observations for the phase intervals 0.85–0.97 and 0.04–0.09. A partially successful attempt was made to reduce this discrepancy by considering a disk with an elliptical cross-section in the orbital plane, with greater extent on the leading edge of the primary than on the trailing edge. However, the additional parameters required reduced the significance of the modeling technique and led to a geometrical complexity unwarranted by the physical assumptions of the model. What is needed is a model based on hydrodynamical calculations, using proper physics and incorporating the possible flow of gas between the stars as well as around the primary.

It is a pleasure to thank Drs. A. H. Batten, C. D. Scarfe, and C. T. Bolton for their advice and encouragement during the course of this work. I would also like to thank Dr. K. O. Wright for permission to use the facilities of the DAO and for the allotment of observing time. Financial support from the National Research Council of Canada is gratefully acknowledged.

REFERENCES

Andersen, J. 1973, *Pub. A.S.P.*, **85**, 191.
Baldwin, B. W. 1976, Ph.D. thesis, University of Victoria.
Batten, A. H. 1970, *Pub. A.S.P.*, **82**, 1.
———. 1973, in *Extended Atmospheres and Circumstellar Matter in Spectroscopic Binary Stars*, ed. A. H. Batten (Dordrecht: Reidel), p. 1.
Batten, A. H., Crampton, D., Fletcher, J. M., and Morbey, C. L. 1971, *Pub. Dom. Ap. Obs., Victoria*, **13**, No. 19.
Beyer, M. 1928, *Astr. Nach.*, **234**, 85.
Castor, J. I. 1970, *M.N.R.A.S.*, **149**, 111.
Castor, J. I., and Van Blerkom, D. 1970, *Ap. J.*, **161**, 485.
Cillié, G. G. 1932, *M.N.R.A.S.*, **92**, 820.
———. 1936, *M.N.R.A.S.*, **96**, 771.
Graff, K. 1931, *Beob. Zirk.*, **13**, 35 (19).
Hiltner, W. A. 1946, *Ap. J.*, **104**, 400.
Iben, I. 1965, *Ap. J.*, **141**, 993.
Koch, R. H. 1970, in *Mass Loss and Evolution in Close Binaries*, ed. K. Gyldenkerne and R. M. West (Copenhagen: Copenhagen University Observatory), p. 85.
Krzemiński, W., and Kraft, R. P. 1964, *Ap. J.*, **140**, 921.
Mihalas, D. 1974, *A.J.*, **79**, 1111.
Nijland, A. A. 1908, *Astr. Nach.*, **178**, 398.
———. 1910, *Astr. Nach.*, **183**, 281.
———. 1927, *Astr. Nach.*, **229**, 345.
Nijland, A. A. 1928, *Acta Astr.*, Ser. C, **1**, 29.
———. 1929, *Astr. Nach.*, **235**, 291.
———. 1931, *Astr. Nach.*, **242**, 23.
———. 1932, *Astr. Nach.*, **245**, 149.
———. 1933, *Astr. Nach.*, **249**, 1.
———. 1934, *Astr. Nach.*, **252**, 69.
———. 1936, *Astr. Nach.*, **259**, 69.
Plavec, M. 1968*a*, *Adv. Astr. Ap.*, **6**, 201.
———. 1968*b*, *Bull. Astr. Inst. Czechoslovakia*, **19**, 11.
———. 1970, *Pub. A.S.P.*, **82**, 957.
Popper, D. M. 1975, private communication.
Roxburgh, I. W. 1966, *A.J.*, **71**, 133.
Seares, F. H. 1908, *Laws Obs. Bull.*, Vol. **16**.
Shapley, H. 1913, *Astr. Nach.*, **194**, 225.
Sobolev, V. V. 1947, *Moving Envelopes of Stars* (Cambridge: Harvard University Press).
———. 1960, *Soviet Astr.—AJ.*, **3**, 735.
Struve, O. 1944, *Ap. J.*, **99**, 89.
Szafraniec, R. 1960, *Ecl. Binaries Circ.*, No. 21 (Cracow Obs).
———. 1962, *Acta Astr. Suppl.*, **5**, 573.
Wright, K. O. 1970, *Vistas in Astronomy*, **12**, 147.
Wyse, A. B. 1934, *Lick Obs. Bull.*, **17**, 37.
Yamasaki, A. 1971, *Publ. Astr. Soc. Japan*, **23**, 33.
Zinner, E. 1932, *Veröff. Remeis-Sternw. Bamberg*, **1**, no. 3.

BARROW W. BALDWIN: David Dunlap Observatory, Box 360, Richmond Hill, Ontario, Canada L4C 4Y6